Journal of Materials Chemistry A

Accepted Manuscript

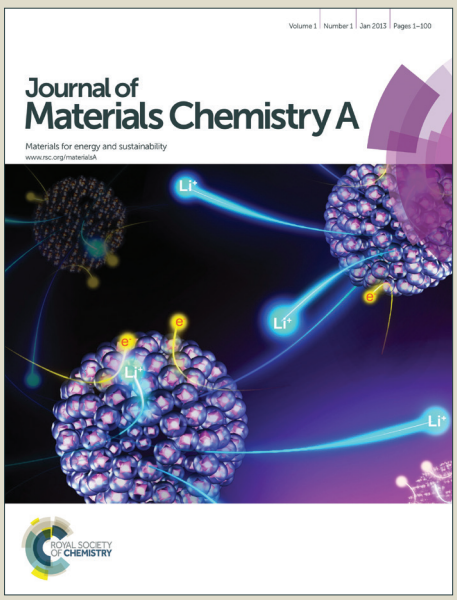

ROYAL SOCIETY OF CHEMISTRY

www.rsc.org/materialsA

Low-Temperature, Solution-Deposited Metal Chalcogenide Films as Highly Efficient Counter Electrodes for Sensitized Solar Cells

Feng Liu,[1] Jun Zhu,[*,1] Linhua Hu,[1] Bing Zhang,[2] Jianxi Yao,[2] Md. K. Nazeeruddin,[3] Michael Grätzel,[*,3] and Songyuan Dai[*,1,2]

[1]Key Laboratory of Novel Thin Film Solar Cells, Institute of Plasma Physics, Chinese Academy of Sciences, Hefei, 230031, P. R. China

[2]Beijing Key Laboratory of Novel Thin Film Solar Cells, State Key Laboratory of Alternate Electrical Power System with Renewable Energy Sources, North China Electric Power University, Beijing, 102206, P. R. China

[3]Laboratory for Photonics and Interfaces, Institute of Chemical Sciences and Engineering, School of Basic Science, Swiss Federal, Institute of Technology, CH-1015 Lausanne, Switzerland

The transition metal chalcogenide crystalline films, $FeSe_2$, $Cu_{1.8}S$, and CuSe have been deposited from solution by drop casting their dissolved inks onto a conductive substrate, followed by a mild thermal treatment. We demonstrate the resulting chalcogenide films exhibit excellent catalytic activity and function as highly efficient counter electrode (CE) for dye- and quantum dot-sensitized solar cells (DSCs, QDSCs). In particular, $FeSe_2$ and CuSe films produced herein with novel morphologies show better catalytic activity than that of the conventional Pt coated CE used in DSCs and Cu_2S in QDSCs, respectively. Ensuing devices present an improved photovoltaic performance with maximum values of 9.10% for DSCs and 4.94% for QDSCs, comparable to those based on Pt and Cu_2S CEs. The efficient CE materials developed from such a facile and scalable route here offer strong potential for a broader solar cell application that requires low-cost and large-scale production.

Keywords: chalcogenide films; solution processing technology; efficient counter electrode; dye-sensitized solar cell; quantum dot-sensitized solar cell

1. INTRODUCTION

Dye- and quantum dot-sensitized solar cells (DSCs, QDSCs) are a new class of thin-film solar cells that have seen rapid advances in recent years and have attracted considerable attention in both scientific research and commercial applications.[1, 2] The challenge remains, however, especially under

the context of the rapidly developed perovskite solar cells.[3-5] The renaissance of the sensitized solar cells requires their component materials to be highly efficient and cost-effective.[6, 7] Counter electrode (CE) constitutes one of the most important components in both DSCs and QDSCs. Yet the noble metal platinum (Pt), which has long served as the catalyst of choice for triiodide reduction in DSCs increases the cost of the solar cells. Hence, further development of CEs with alternatives being less expensive and more efficient compared to Pt is warranted to boost their photovoltaic performance and to reduce the cost of production. Instead of the cost issues that are encountered by DSCs, CE materials used in QDSCs mainly suffer from mechanical instability problems observed with polysulfide redox system caused by a continual corrosion in the electrolyte, especially for those CEs built on a metal foil substrate.[8, 9] Thus, there is still an urgent need to develop more stable and efficient CEs for QDSCs.

A considerable number of inorganic materials, for instance, WC,[10] VC-MC,[11] TiN-C,[12] NiO,[13] Mo(Co)S_2,[14, 15] $Ni_{0.85}(Co_{0.85})Se$,[16, 17] Cu_2S,[8, 18] CuS/CoS,[8, 19-22] PbS,[8, 23, 24] NiS,[25, 26] Ni_3S_2,[27] Bi_2S_3,[28] $NiTe_2$,[29] Ni(Co)MoS_4,[30] CZTS(Se),[31-34] CuS_xSe_{1-x},[35] carbon-, polymer- and graphene-based materials[36-42] have shown their excellent catalytic activity toward the reduction of the oxidized species in either or both of the two above-mentioned electrolytes based either on iodide or sulfide redox electrolytes. These studies undoubtedly provided new insights into the development of Pt-free alternatives in both DSCs and QDSCs. However, most of these inorganic metal compounds may still be plagued by a time and energy-consuming fabrication process hindering their further use for a large-scale application. By contrast, the inexpensive solution processing techniques, including sol-gel-based coating,[43] chemical/electrochemical deposition,[27, 44] spray pyrolysis,[18, 45] and electroplating[8] have shown their remarkable potential for enabling those semiconductors of great electrical or photoelectrical interest to become more widely adopted in photoelectrochemical solar cells that require high performance and low cost.

In this study, we developed solution-processable transition metal chalcogenide crystalline films, environmental friendly $FeSe_2$, $Cu_{1.8}S$, and CuSe films comprised of earth-abundant elements having extremely high catalytic activity. These CE materials were readily prepared on a conductive substrate via an extremely facile solution-phase deposition process by using their dissolved precursor inks,

followed by a mild thermal treatment, thereby being processable in large-scale production. The precursor inks were prepared by dissolving the parent chalcogenides (FeSe, $Cu_{1.9}S$, Cu_2Se) in a binary solvent mixture comprised of ethanedithiol and ethylenediamine, which was introduced by Brutchey's group.[46] Solid materials of these compositions are recovered from the heat treatment of the above solutions. We demonstrate that the resulting films ($FeSe_2$, $Cu_{1.8}S$, and CuSe) can serve as highly efficient CEs for DSCs and QDSCs.

In the following, we shall first show the amazing solubility of these three investigated materials in the binary solvent mixture, and then characterize the crystalline quality as well as the surface morphology of the obtained films by means of X-ray powder diffraction (XRD) and scanning electron microscopy (SEM). The catalytic activity of the chalcogenide films as CE catalytes in DSCs and QDSCs was rigorously examined by several electrochemical methods, i.e. cyclic voltammetry, impendance spectra, and Tafel polarization. It is noteworthy that the so prepared $FeSe_2$ and CuSe films with novel morphologies exhibited an excellent ability to catalyze electron exchange between the TCO glass and the redox electrolyte in DSCs and QDSCs, respectively, comparable to those based on Pt and Cu_2S CEs, yielding robust and high-performance solar cells.

2. EXPERIMENTAL DETAILS

2.1 Materials. FeSe (99.99%), $Cu_{1.9}S$ (99.5%), and Cu_2Se (99.5%) powders were purchased from Alfa Aesar. 1,2-ethanedithiol was purchased from J&K Chemical (Beijing, China) and 1,2-ethylenediamine was purchased from Sinopharm Chemical Reagent (Shanghai, China). All of the reagents were used as received.

2.2 Preparation of Counter Electrodes. $Cu_{1.9}S$, FeSe, and Cu_2Se precursor solutions used here with a maximum soluble concentration of 0.4 M, 0.3 M, 0.4 M respectively were prepared by directly dissolving the as-bought powders into a solution composed of 5 mL 1,2-ethylenediamine and 0.5 mL 1,2-ethanedithiol in a sealed bottle at 60 ℃ assisted by sonication for ca. 5 h. $Cu_{1.8}S$, $FeSe_2$, and CuSe CEs were obtained by drop-casting 50 μL of the above dissolved precursor solutions onto a fluorine-doped tin oxide (FTO) glass substrate (1.5 cm × 2 cm), followed by an annealing process to recover the solids. The annealing conditions were guided by the TGA results (Supporting Information,

Figure S1). In an evacuated fused silica tube under flowing nitrogen, solutions were firstly heated to 110 ℃ to dry for 10 min, then ramped (10 ℃/min) to a final temperature 330 ℃, where they were kept for another 10 min. The samples were subsequently allowed to naturally cool down to room temperature. Brass-based Cu_2S CE was prepared according to Hodes et al.'s method.[8] Typically, the polished brass foils were immersed in HCl (37%) solution at 70 ℃ for 5 min and subsequently washed with water, then followed by sulfidation in polysulfide solution (1 M S, 1 M Na_2S in water).

2.3 Fabrication of Liquid Junction QDSCs and DSCs. TiO_2 mesoporous films (18 μm thick) composed of a transparent (12 μm) and superimposed light-scattering layer (6 μm) were prepared for both QDSCs and DSCs according as previously reported.[47] CdSe QD-sensitized TiO_2 photoanodes were prepared via a typical SILAR method according to Lee et al..[48] Briefly, the mesoporous TiO_2 films were dipped alternatively into solutions of 0.3 M $Cd(NO_3)_2$ and 0.3 M Na_2Se in a nitrogen-filled glove box. The dipping cycle was repeated 5 times and 6 min was used for each dipping. Dye-sensitized photoelectrodes for DSCs were prepared by soaking the TiO_2 films in a 0.3 mM Na-Ru(4,1'-bis(5-hexylthiophen-2-yl)-2,2'-bipyridine)(4-carboxylic-acid-4'-carboxylate-2,2'-bip-yridine) $(thiocyanate)_2$ (C101 dye, which was kindly provided by Prof. Peng Wang) solution in acetonitrile overnight at room temperature. The polysulfide electrolyte was prepared by dissolving sulfur powder in an aqueous Na_2S and KCl solution (1 M S, 1 M Na_2S, and 0.1 M KCl) under vigorous stirring. The electrolyte used for DSCs contained 0.03 M I_2, 0.06 M LiI, 0.5 M *tert*-butylpyridine, 0.6 M 1-butyl-3-methylimidazolium iodide, and 0.1 M guanidinium thiocyanate in anhydrous acetonitrile. The sandwich-type solar cells were fabricated by placing counter electrode on a sensitized TiO_2 photoanode using a thermal adhesive film (Surlyn, 60 μm, Dupont). The electrolyte solution was then injected by vacuum backfilling followed by a sealing procedure with a Surlyn film and a cover glass under heat. The active surface area of the mask-covered solar cells was measured to be 0.25 cm^2.

2.4 Characterizations.

Thermo-gravimetric analysis (TGA) was carried out on a TGA Q5000IR equipment (TA Instruments, USA). XRD spectra were obtained on an X-ray diffraction analysis instrument with Cu Kα irradiation (λ = 0.154 nm) (TTR-III, Rigaku Corp., Japan). The surface morphology of the CE films was observed

by field emission scanning electron microscopy (FESEM, FEI, Quanta 200FEG). The cyclic voltammetry (CV) measurement was performed with a three-electrode system at a scan rate of 20 mV s^{-1} using an argon-purged electrolyte solution for $Cu_{1.8}S$ and CuSe CV measurements, ultrapure aqueous solutions of 1 M S and 1 M Na_2S were prepared as the electrolyte, a Pt mesh used as the counter electrode, a saturated calomel electrode (SCE) as the reference electrode and the chalcogenides coated FTO glass as the working electrode. For $FeSe_2$, the CV electrolyte contains 0.1 M $LiClO_4$, 10 mM LiI, and 1 mM I_2 in acetonitrile, an Ag/Ag^+ electrode serving as the reference electrode. Electrochemical impedance spectroscopy (EIS) was carried out on a symmetrical dummy cell at an applied bias of 0 V the modulation frequency ranging from 0.1 Hz to 500 kHz, with a 5 mV ac amplitude. Tafel polarization curves were also measured on the dummy cells with a scan rate of 50 mV s^{-1}. The latter were prepared by sandwiching two identical electrodes with the same redox electrolyte as used in the solar cells filled in-between. The geometric surface area of the symmetrical cells was 0.56 cm^2. The BET specific surface area of the CE films was measured with a nitrogen adsorption-desorption apparatus (Tristar 3020, Micromeritics). All the electrochemical measurements were conducted on an electrochemical workstation (Autolab 302N, Metrohm, Switzerland). *J-V* characteristics of the solar cells were derived with a Keithley 2420 digital source meter (Keithley, USA) under a 450W xenon lamp (Oriel Sol3A Solar Simulator 94043, Newport Stratford Inc., USA).

3. RESULTS and DISCUSSION

3.1 Characterizations of the Metal Chalcogenide Films by XRD and SEM. Figure 1 shows the photographs of solutions of FeSe, $Cu_{1.9}S$, and Cu_2Se. The coloration is red, light brown and dark brown for FeSe, $Cu_{1.9}S$ and Cu_2Se, respectively. It is noted that chalcogenide solutions can be stored under ambient condition, yet they should be used within one week for FeSe and two weeks for Cu_2Se and $Cu_{1.9}S$. The crystallographic phases of the obtained chalcogenides were investigated by XRD measurement. XRD patterns of the as-bought materials and the powders recovered from solutions were shown in Figure 2-4. It was observed that the main diffraction peaks of the as-bought powders are in identical positions of the standard XRD database, i.e. monoclinic phase $Cu_{1.9}S$ (PDF no. 34-0660); tetragonal phase FeSe (PDF no. 85-0735); monoclinic phase Cu_2Se (PDF no. 27-1131).

However, the XRD patterns of the solution-recovered samples differed from those of the as-bought materials, i.e. $Cu_{1.8}S$ (hexagonal phase, PDF no. 23-0962), $FeSe_2$ (orthorhombic phase, PDF no. 74-0247), and CuSe (hexagonal phase, PDF no. 27-0185) of high-crystallinity and pure-phase were identified for the resulting materials, indicating phase as well as stoichiometry change during the recovering process. The observed phenomenon related to the material transition from the parent to the annealed material is quite different from that of Brutchey et al.'s study in which the same phase and same stoichiometry are recovered after annealing.[46, 49] In fact, heat treatment only, without dissolving in the binary solvent, causes neither phase nor stoichiometry change, for example, on the as-bought $Cu_{1.9}S$ powder, as was shown in Figure 2c. We consider the possible reason for this compositional change in our case can be due to the partial oxidation of the materials during their dissolution in the solvent, for example, Cu^+ being oxidized to Cu^{2+}, Fe^{2+} being oxidized to Fe^{3+}. The other consideration, is that the partial evaporation with loss of metallic elements (Cu, Fe) during the sintering process. The first explanation seems like to be more plausible since in our study the dissolution of these materials in the mixed solvent was carried out in open air under ambient conditions and all prepared precursor solutions were stored in air before use, while in Brutchey et al.'s study, the whole procedure, from the preparation of the precursor solutions until the recovery of the films, was conducted under nitrogen.[46, 49] Yet we can not state with certainty the cause of such a change in the absence of more complete data.

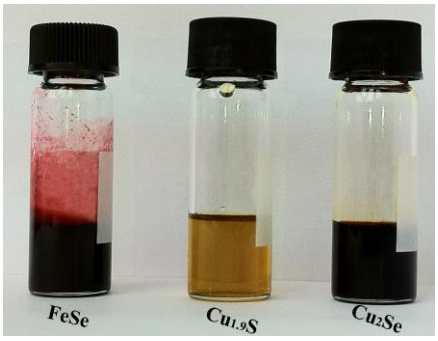

Figure 1. Photographs of precursor solutions of FeSe, $Cu_{1.9}S$, and Cu_2Se in the solvent mixture.

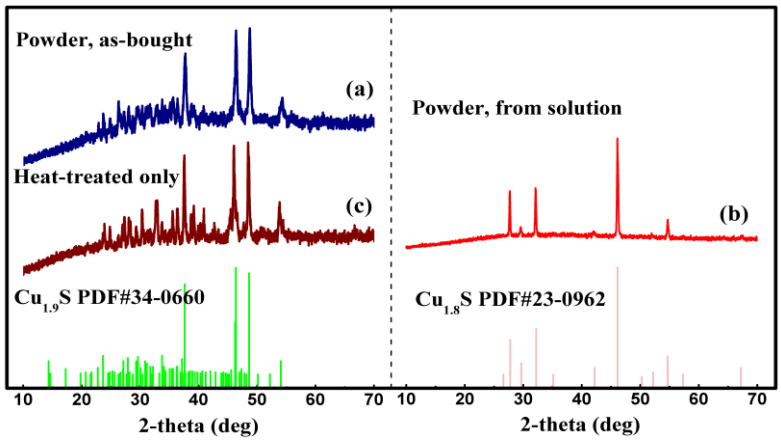

Figure 2. XRD patterns of (a) the as-bought $Cu_{1.9}S$ powder and (b) the powder recovered from solution by a heat treatment at 330 ℃. (c) XRD patterns of the as-bought $Cu_{1.9}S$ powder that underwent the same procedure of heat treatment for sample (b).

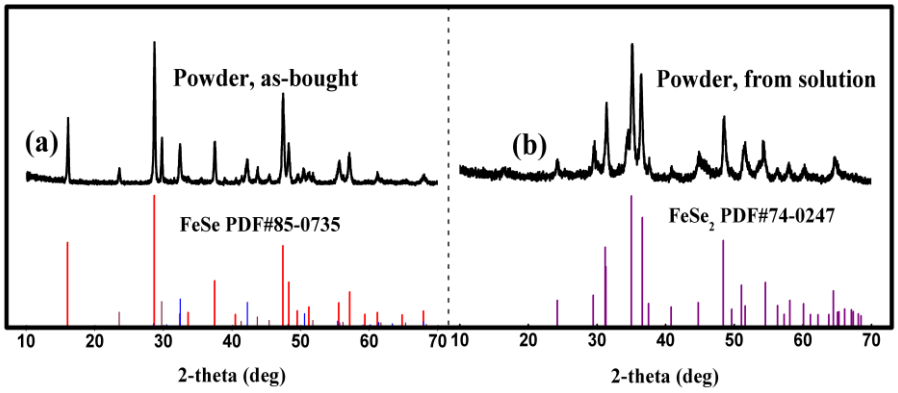

Figure 3. XRD patterns of (a) the as-bought FeSe powder and (b) the powder recovered from solution by a heat treatment at 330 ℃. Peaks of small amounts of impurities like hexagonal phase FeSe (PDF no. 75-0608) and Se (PDF no. 06-0362) were identified in the as-bought material.

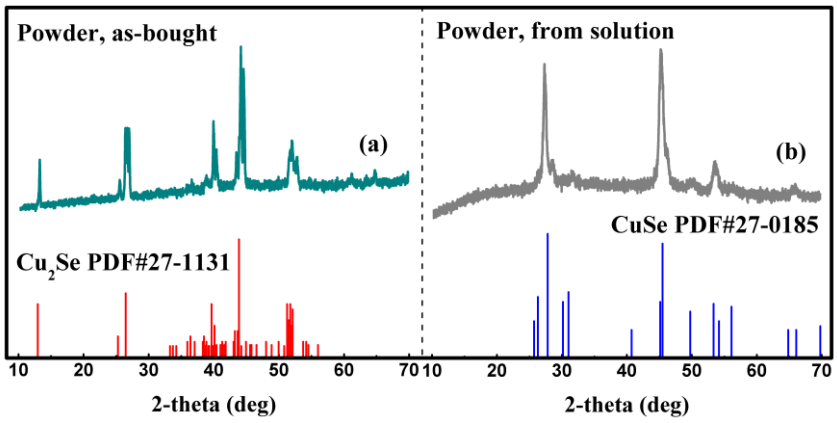

Figure 4. XRD patterns of (a) the as-bought Cu_2Se powder and (b) the powder recovered from solution by a heat treatment at 330 ℃.

The morphology of the three chalcogenide films solution-cast on FTO glass was investigated using SEM. Cross-sectional SEM images (Figure S2, Supporting Information) reveal a ~25 μm film thickness for $FeSe_2$, while a thicker film thickness of $Cu_{1.8}S$ and CuSe was obtained with uniform chalcogenide layer composed of large grains fully covers the surface of FTO substrate. No major microscopic cracks or pinholes were observed for the resulting films. It is important to note that these chalcogenide films were strongly bound to the FTO substrates, and sonication in electrolyte solution for 1 h was not able to peel them off, suggesting the good mechanical stability of prepared CEs. Higher-resolution top-view images revealed a similar porous microstructure for the obtained films whilst distinct morphology features appear for each film. Micrometer-sized clusters comprised of loosely arranged disk-like sheets (irregular shape of 250 nm~300 nm size) were observed for the resulting $FeSe_2$ (Figure 5a, b) and $Cu_{1.8}S$ (Figure 5c, d) products with $FeSe_2$ exhibiting somewhat thicker and larger particles than $Cu_{1.8}S$; while in the case of CuSe (Figure 5e, f), smaller sheets (size ~100 nm) were found to form densely packed clusters. We note that although there are a few differences in shapes obtained for these three different materials, yet they are not so big. We consider the main reason for this interesting observation is that the different materials were prepared through an identical solution-phase preparation procedure and we believe both of the morphology and shape of the resulting films should be closely related to the preparation approach that employed. Specifically, solid parent materials were dissolved in the same solvent and thin film products were obtained by the same heat treatment of the dissolved inks. More importantly, preliminary investigation on the composition and nature of the dissolved metal chalcogenides implied that these different materials share the same dissolution and stabilization mechanism, forming similar formula and molecular structure in the ethanedithiol and ethylenediamine solvent system.[46] It has been demonstrated that apart from the intrinsic catalytic property of the material, the difference in electrode morphology should also be responsible for the variation in catalytic activity.[50] The highly porous microstructure of the resulting films yields electrodes with large specific surface area (average values of 22.5, 29.3, 24.0

$m^2\ g^{-1}$ for $FeSe_2$, CuSe, and $Cu_{1.8}S$, respectively) and thus undoubtedly helps to provide more catalytic active sites for the redox process. Specifically, theoretical studies have suggested a great dependence of the catalytic property on the morphology of a given electrode,[51] and in fact a higher catalytic activity was observed in thicker and more porous electrodes by Aksay et al..[50] Solution processing technologies offer a distinct advantage such as the direct and easy control of the thickness of the films. Here the film thickness of the chalcogenides can be easily controlled by varying either the solution concentration or the number of coating (data not shown). Although the optimization of the chalcogenide cathodes (e.g., thickness) is beyond the scope of this present work, we note that, in guarantee under the premise of the good adhesion between the loaded films and the substrate, higher surface coverage and thicker coating thickness of the chalcogenide films on FTO glass are both helpful for obtaining CEs of high performance.

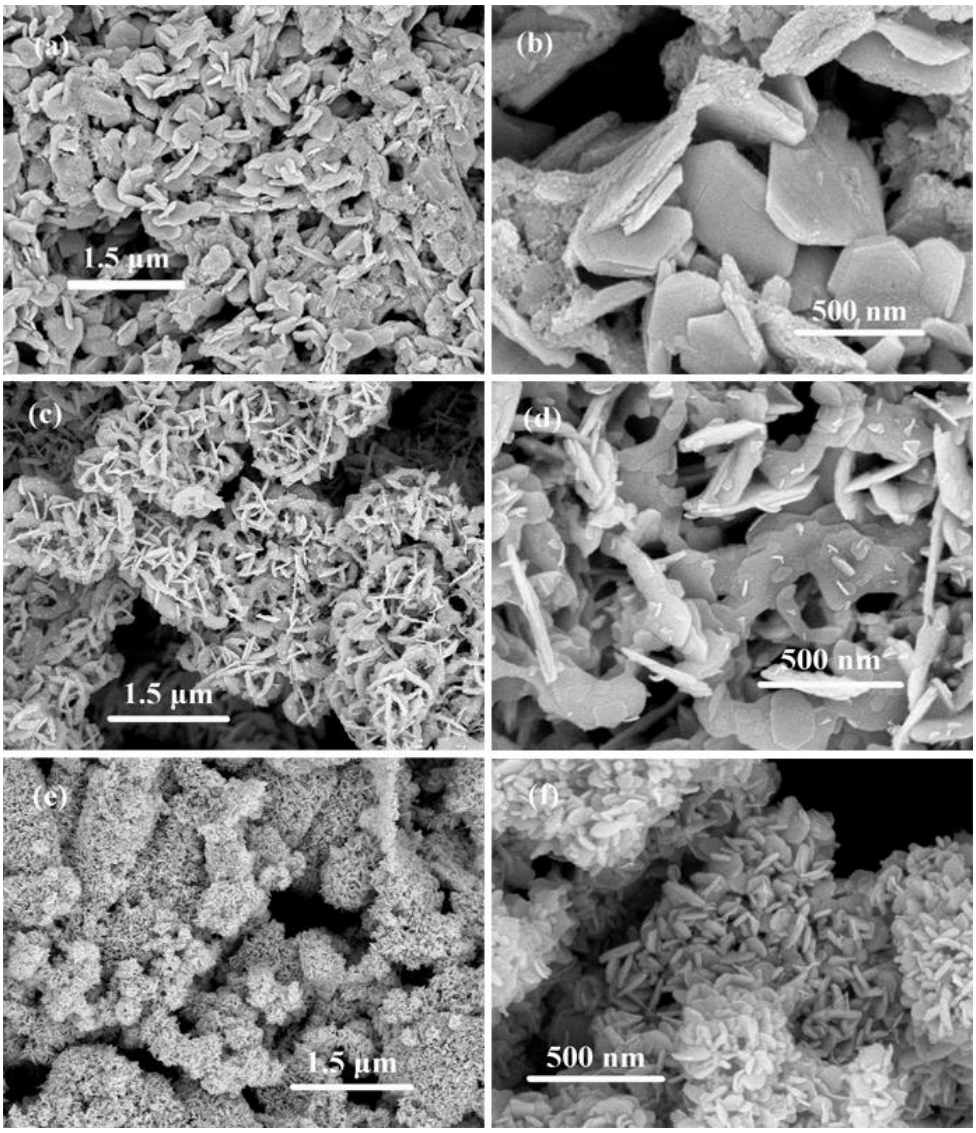

Figure 5. Top-view images of (a, b) $FeSe_2$, (c, d) $Cu_{1.8}S$, and (e, f) CuSe films.

3.2 Investigations of the Catalytic Activities of the Chalcogenides ($FeSe_2$, CuSe, $Cu_{1.8}S$) Loaded CEs by CV, EIS, and Tafel Polarization Tests. The redox processes at the electrode/electrolyte interface were probed by means of cyclic voltammetry measurement. Figure 6a presents the cyclic voltammograms of iodide/triiodide redox species for the $FeSe_2$ and Pt electrodes. The cycling was performed 10 times at a scan rate of 20 mV s^{-1} and no significant changes were observed in both curve shape and peak current density, suggesting a good electrochemical stability of $FeSe_2$ CEs during the redox process. It is seen that both of the electrodes exhibit two pairs of oxidation-reduction peaks (Ox'/Red', Ox''/Red'', as labeled in Figure 6a). The left and right pairs are assigned to the redox

reaction of I^-/I_3^- and I_2/I_3^-, which can be described by eqn (1) and (2), respectively. Since the CE is responsible for catalyzing the reduction of I_3^- to I^-, the characteristics of peaks Ox'and Red' are the focus of our analysis. It is observed that the cathodic and anodic peak currents with $FeSe_2$ CE are slightly higher than that of Pt, indicating that the $FeSe_2$ material has better electrocatalytic activity than Pt. In addition, the peak to peak separation value (ΔE_p) as labeled in Figure 6a, which correlates with the standard electrochemical rate constant of the redox reaction, is smaller in the case of $FeSe_2$ (average value of 258 mV, compared with the Pt value of 337 mV), signifying its higher catalytic activity toward the reduction of triiodide. In fact, the good catalytic performance of the $FeSe_2$-based CEs has been demonstrated in our previous study where $FeSe_2$ particles were in-situ grown on a FTO glass and they exhibited a completely distinct morphology from these solution-deposited CE films.[52]

$$I_3^- + 2e^- \leftrightarrow 3I^- \qquad (1)$$

$$3I_2 + 2e^- \leftrightarrow 2I_3^- \qquad (2)$$

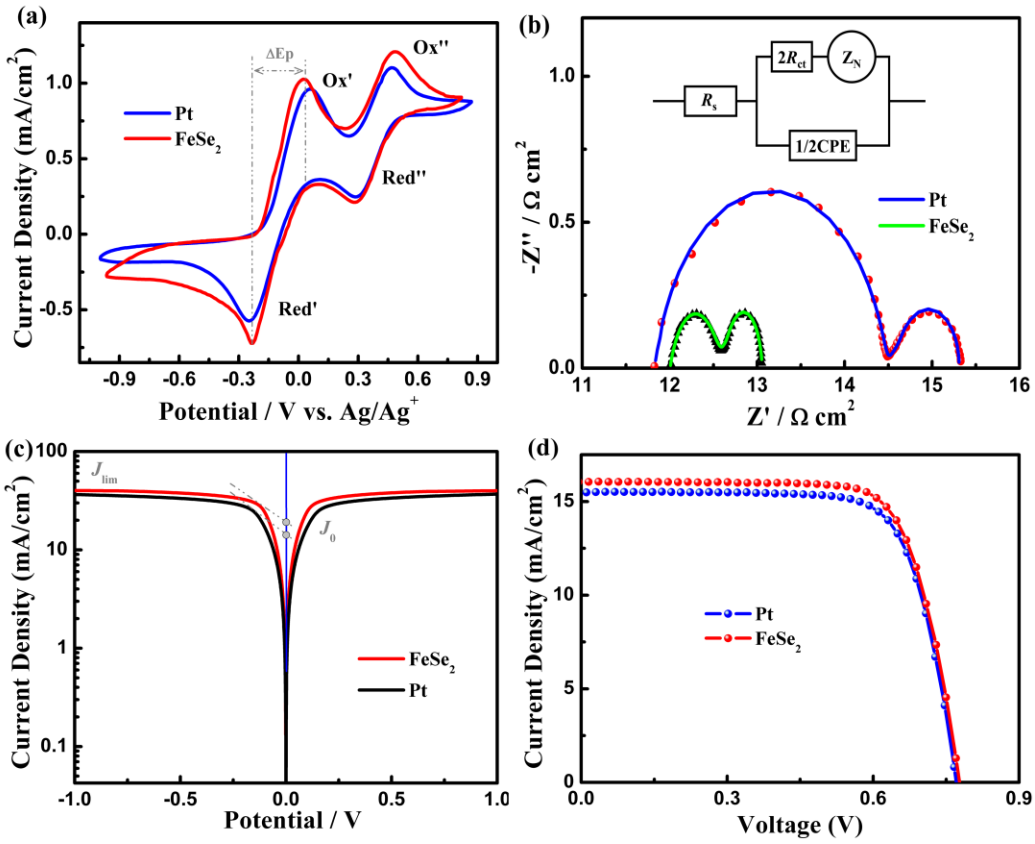

Figure 6. (a) CV curves of iodide/triiodide redox species for $FeSe_2$ and Pt electrodes. (b) Nyquist

plots of EIS for $FeSe_2$ and Pt thin-layer symmetrical cells. The inset shows the equivalent circuit used to fit the EIS spectra. (c) Tafel polarization curves of the symmetrical cells, measured at 20 ℃. (d) *J-V* curve characteristics of DSCs with $FeSe_2$ and Pt CEs.

Table 1. Photovoltaic Performance of the DSCs with Different CEs and the Fitted EIS Parameters Extracted from the Corresponding Symmetric Cells[a]

CE	V_{oc}/mV	J_{sc}/mA cm^{-2}	FF	PCE/%	R_s/Ω cm^2	R_{ct}/Ω cm^2	Z_N/Ω cm^2	ΔE_p/mV
$FeSe_2$	753±1	16.06±0.05	0.74±0.01	9.01±0.09	12.15±0.65	0.18±0.01	0.25±0.02	258±20
Pt	751±2	15.58±0.20	0.72±0.01	8.42±0.13	11.82±0.80	0.72±0.01	0.40±0.01	337±7

[a]The data shown are the average values obtained from 4 devices with standard deviation. See Table S1 (Supporting Information) for individual solar cell characterization in each set.

EIS measurement was further carried out to scrutinize the catalytic activity of the $FeSe_2$ loaded electrodes. Figure 6b shows the Nyquist plots obtained from the $FeSe_2$ and Pt symmetrical thin-layer cells. The electrochemical parameters of the symmetrical cells extracted by fitting the EIS spectra are summarized in Table 1. It was found that the charge transfer resistance (R_{ct}) for $FeSe_2$ CE at the electrode/electrolyte interface was less than that of Pt CE, showing a better catalytic performance of $FeSe_2$. In addition, the Nernst diffusion-limited impendence (Z_N), which can be calculated by eqn (3), exhibits a smaller value for the one with $FeSe_2$ CE, implying a larger diffusion coefficient in the case of $FeSe_2$ CE and, thus, a higher catalytic activity since the diffusion rate of the iodide species has a positive correlation with the reduction rate of the triiodide on the surface of the catalyst. The photovoltaic performance (Figure 6d, summarized in Table 1) of two representative integrated solar cells comprised of dye-sensitized photoanodes and Pt or $FeSe_2$ CEs in iodide electrolyte is consistent with that predicted from electrochemical measurements. In addition, to demonstrate the durability and reproducibility of the prepared $FeSe_2$ CEs, we present the photovoltaic device characteristics measured for solar cells assembled with photoanodes from different batches and a reused $FeSe_2$ CE in Table S2 (Supporting Information). We found that solar cells fabricated with reused CE exhibited near-identical efficiencies, indicating high reproducibility and stability of the $FeSe_2$ CE in iodine-based electrolyte.

$$Z_N = \frac{kT}{n^2 e_0{}^2 cA\sqrt{i\omega D}} \tanh\left(\sqrt{\frac{i\omega}{D}}\delta\right) \qquad (3)$$

where k is the Boltzmann constant, T the temperature, n the electron number involved in the reaction, e_0 the elementary charge, c the concentration of triiodide, A the effective electrode area, ω the angular frequency, D the diffusion coefficient of triiodide and δ is the thickness of the diffusion layer.

To reconfirm the excellent electrochemical characteristics of the $FeSe_2$ films in iodide-based electrolyte, Tafel polarization curves on symmetrical cells were also measured. Figure 6c shows the current density as a function of voltage for the iodide electrolyte in $FeSe_2$ symmetrical cells, a Pt assembled symmetrical cell was also measured for comparison. Both systems behave reversibly. The anodic and cathodic branches of the Tafel curve of the $FeSe_2$ loaded electrode show larger slopes than those obtained with Pt, revealing a higher exchange current density (J_0) on the electrode. J_0 can be expressed by eqn (4), one can see that J_0 varies inversely with R_{ct}. The variation of J_0 derived from the Tafel curve is in fair agreement with the above EIS results concerning the R_{ct} value, reconfirming the smaller charge transfer resistance on the $FeSe_2$ deposited electrode. In addition, the limiting current density (J_{lim}) of the symmetrical cells, which is determined by diffusion velocity of the ionic carriers (mainly triiodide) between the two electrodes and the catalytic properties of the CE materials, can be also derived from the Tafel polarization measurement. J_{lim} is given by eqn (5) and it can be seen that the case with $FeSe_2$ electrode gives a higher J_{lim} value as compared to the one with Pt, suggesting a larger diffusion coefficient of the triiodide, which is also consistent with the results on D value that revealed by EIS spectra.

$$J_0 = \frac{RT}{nFR_{ct}} \qquad (4)$$

$$J_{lim} = \frac{2ncFD}{l} \qquad (5)$$

where R is the gas constant, F the Faraday's constant, and R_{ct} is the charge transfer resistance, l is the spacer thickness, T, D, c and n retain their established meanings.

So far, we have shown the excellent catalytic activity of the solution-processed $FeSe_2$ films in the iodide/triiodide-based electrolyte for DSCs. Next, we shall show the deposited $Cu_{1.8}S$ films on FTO

glass and demonstrate their superior catalytic activity toward the reduction of polysulfide in QDSCs. In addition, the catalytic activity and the electrochemical stability of the newly developed CuSe CE materials in polysulfide-based electrolyte were also investigated.

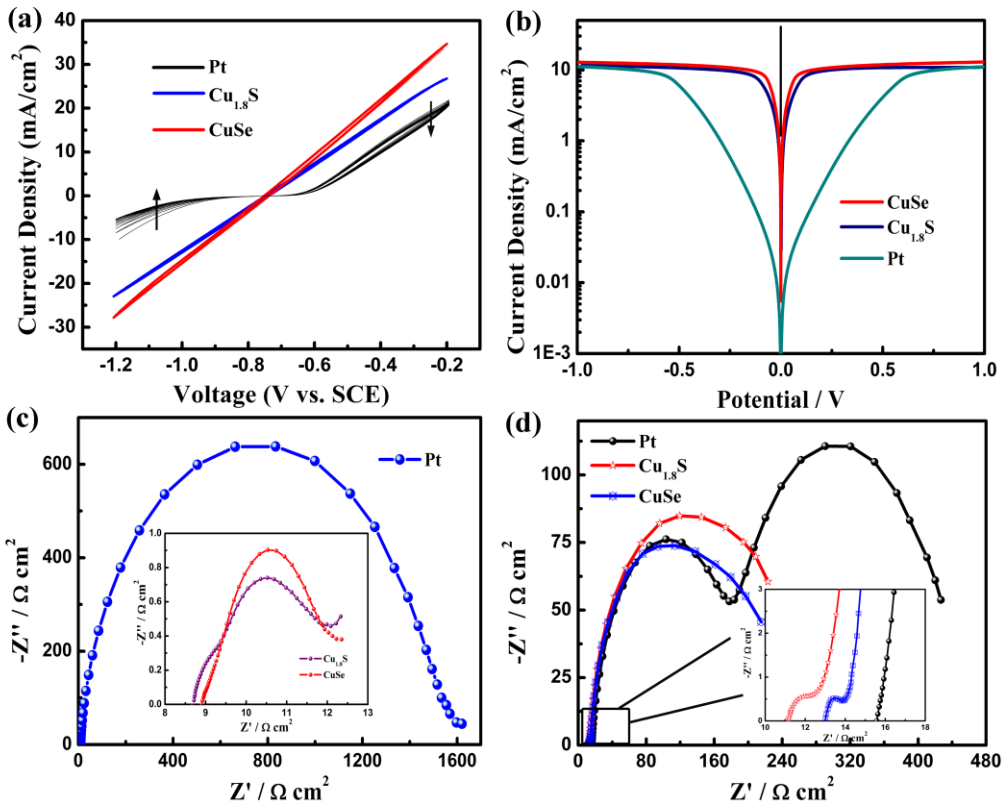

Figure 7. (a) Cyclic voltammograms for the $Cu_{1.8}S$, CuSe, and Pt electrodes. (b) Tafel polarization curves of the symmetric cells. (c) EIS of the symmetric cells. (d) EIS of a complete solar cell, measured in the dark under a forward bias of -0.55 V. The frequency ranged from 0.07 Hz to 100 KHz and the ac modulation amplitude was a 5 mV.

Figure 7a shows the results of the CV test on Pt, $Cu_{1.8}S$, and CuSe electrodes. We note that, in QDSCs, similar CV behavior of CEs in polysulfide redox system was observed in other reports.[8, 9, 21] Ten consecutive cycles were performed on $Cu_{1.8}S$ and CuSe electrodes and there was negligible change in both curve shape and current density, suggesting the good electrochemical stability and reproducible cycling behavior of $Cu_{1.8}S$ and CuSe films in the electrolyte. However, the current density of the Pt electrode rapidly decayed upon repeated cycling to approximately half of its initial value after 10 cycles. This is caused by the fact that sulfur compounds can chemisorb on platinum

surface and induce poisoning effects toward electrode activity.[53] It is observed that at the reduction zone CuSe displays current densities that are 8 to 10 times greater than that of Pt electrode and even higher than $Cu_{1.8}S$ films, demonstrating its superior catalytic activity toward the reduction of polysulfide. It is interesting to note that both of the $Cu_{1.8}S$ and CuSe films yield the current density at all potentials comparable to that of the graphene oxide-Cu_2S composite, an outstanding CE material introduced by Kamat et al. for the reduction of polysulfide.[9] The advantage of CuSe films as catalytic CE can also be demonstrated by Tafel polarization measurement. As shown in Figure 7b, a larger slope in the anodic or cathodic branch was observed in the case of CuSe, indicating a higher J_0 on the electrode, and thus revealing a smaller R_{ct} value for the CuSe CE according to eqn (4). To elucidate the results more accurately, EIS measurement on the symmetric cells was carried out. The resulting Nyquist plots of symmetric cells based on the three CEs are shown in Figure 7c. The high frequency arcs of the three CEs are clearly visible (the inset depicts the enlarged R_{ct} part of the Nyquist plot of $Cu_{1.8}S$ and CuSe) and R_{ct} values of CEs can be extracted by fitting the spectra to the same equivalent circuit as was shown in Figure 6b. The average R_{ct} values for $Cu_{1.8}S$ and CuSe were 0.9 Ω cm^2 and 0.7 Ω·cm^2, respectively, while a quite large average value of 420.2 Ω·cm^2 was obtained for Pt CE, confirming the superb catalytic activity for both $Cu_{1.8}S$ and CuSe films. Impedance measurement was further performed on an integrated cell device to reconfirm the superior catalytic activity of the CuSe films. As was shown in Figure 7d, the radius of the semicircle in the higher frequency region which represents the R_{ct} value at the CE/electrolyte interface increased in the order CuSe < $Cu_{1.8}S$ < Pt, attesting to the inverse order of the electrocatalytic activity that revealed by the above CV, Tafel polarization and impedance analyses on the symmetric cells. A further comparison was made with R_{ct} value obtained from the brass-Cu_2S CE, a commonly used electrocatalyst for highly efficient QDSCs. While EIS spectra (Figure S3, Supporting Information) reveal a smaller R_{ct} value for the CuSe CE, which is indicative of its superior catalytic performance to Cu_2S CE. The results of the above electrochemical measurements thus further explain the observed differences in photovoltaic performance of four representative QDSCs based on the different CEs as summarized in Figure 8 and Table 2. Additionally, to show the good reproducibility and stability of $Cu_{1.8}S$ and CuSe CEs, we have

also presented the photovoltaic performance measured for QDSCs assembled with photoanodes from different batches and a reused CE in Table S4 (Supporting Information).

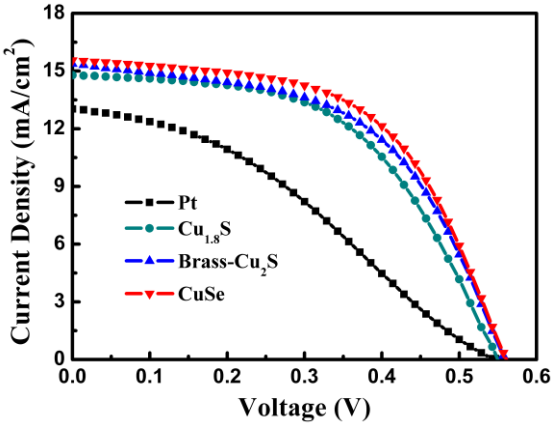

Figure 8. *J-V* curve characteristics of the CdSe-QDSCs with different CEs.

Table 2. Catalytic and Photovoltaic Performance of the CdSe-QDSCs with Different CEs[b]

CE	V_{oc}/mV	J_{sc}/mA cm^{-2}	FF	PCE/%	R_s/Ω cm^2	R_{ct}/Ω cm^2
Pt	545 ±3	13.01 ±0.30	0.35 ±0.03	2.48 ±0.17	8.8 ±0.1	420.2 ±5.9
$Cu_{1.8}S$	550 ±2	14.82 ±0.24	0.53 ±0.01	4.31 ±0.11	8.8 ±0.1	1.2 ±0.1
Brass-Cu_2S	557 ±3	15.31 ±0.12	0.54 ±0.01	4.60 ±0.12	9.1 ±0.1	0.9 ±0.1
CuSe	561 ±1	15.63 ±0.11	0.56 ±0.01	4.89 ±0.06	8.9 ±0.2	0.7 ±0.1

[b]The data shown are the average values obtained from 3 devices with standard deviation. See Table S3 (Supporting Information) for individual solar cell characterization in each set.

4. CONCLUSIONS

In conclusion, three kinds of novel transition metal chalcogenide crystalline films, $FeSe_2$, $Cu_{1.8}S$, and CuSe have been deposited on FTO glass via an extremely facile solution-based method, being processable in large-scale production. Further, we have demonstrated that the resulting chalcogenide films on FTO glass function as highly efficient catalytic CEs for QDSCs and DSCs. Particularly, $FeSe_2$ and CuSe films prepared herein with novel morphologies exhibited better catalytic activity than that of the commonly used Pt and Cu_2S cathodes toward the reduction of the oxidized species in iodide-based and polysulfide-based electrolyte, respectively. Ensuing QDSCs and DSCs based on these highly efficient CE materials produced an improved photovoltaic efficiency with maximum

values of 9.10% for DSCs and 4.94% for QDSCs, comparable to those based on Pt and Cu_2S CEs. Our findings presented here open up a new vista of opportunity for metal chalcogenides to serve as low-cost, earth-abundant, and high-performance catalysts in photo-electrochemical solar cells. Still, it is noteworthy that, though relatively good short-term stability in the electrolyte has been confirmed (e.g., by conducting 10 complete cycles CV measurement and reproducibility measurement) for these proposed CEs, the long-term stability is still needed to be further assessed as this should be of great significance for their practical applications and we will continue to work on this issue.

ASSOCIATED CONTENT

Supplementary Information

TGA curves of FeSe, $Cu_{1.9}S$, and Cu_2Se solid precursors, cross-sectional SEM images, enlarged R_{ct} part of the Nyquist plot of the integrated QDSCs with three different CEs, photovoltaic performance of the DSCs and QDSCs, catalytic performance of the CEs.

AUTHOR INFORMATION

Corresponding Authors

*E-mail: zhujzhu@gmail.com. Tel: +86 0551-65593222.

*E-mail: sydai@ipp.ac.cn. Tel: +86 0551-65591377.

*E-mail: michael.graetzel@epfl.ch. Tel: +41 021-6933112.

Author Contributions

The manuscript was written through contributions of all authors. All authors have given approval to the final version of the manuscript.

Notes

The authors declare no competing financial interest.

ACKNOWLEDGEMENTS

This work was supported by the National Basic Research Program of China under Grant No. 2011CBA00700, the National Natural Science Foundation of China under Grant No. 21403247, 21173228.

REFERENCES

1. Z. X. Pan, I. Mora-Sero, Q. Shen, H. Zhang, Y. Li, K. Zhao, J. Wang, X. H. Zhong and J. Bisquert, *J. Am. Chem. Soc.*, 2014, 136, 9203-9210.
2. S. Mathew, A. Yella, P. Gao, R. Humphry-Baker, B. F. E. Curchod, N. Ashari-Astani, I. Tavernelli, U. Rothlisberger, M. K. Nazeeruddin and M. Gratzel, *Nat. Chem.*, 2014, 6, 242-247.
3. L. Etgar, P. Gao, Z. S. Xue, Q. Peng, A. K. Chandiran, B. Liu, M. K. Nazeeruddin and M. Gratzel, *J. Am. Chem. Soc.*, 2012, 134, 17396-17399.
4. M. Z. Liu, M. B. Johnston and H. J. Snaith, *Nature*, 2013, 501, 395-398.
5. J. A. Christians, R. C. M. Fung and P. V. Kamat, *J. Am. Chem. Soc.*, 2014, 136, 758-764.
6. S. Thomas, T. G. Deepak, G. S. Anjusree, T. A. Arun, S. V. Nair and A. S. Nair, *J. Mater. Chem. A*, 2014, 2, 4474-4490.
7. W. Kwon, J. M. Kim and S. W. Rhee, *J. Mater. Chem. A*, 2013, 1, 3202-3215.
8. G. Hodes, J. Manassen and D. Cahen, *J. Electrochem. Soc.*, 1980, 127, 544-549.
9. J. G. Radich, R. Dwyer and P. V. Kamat, *J. Phys. Chem. Lett.*, 2011, 2, 2453-2460.
10. J. S. Jang, D. J. Ham, E. Ramasamy, J. Lee and J. S. Lee, *Chem. Commun.*, 2010, 46, 8600-8602.
11. M. X. Wu, X. Lin, Y. D. Wang, L. Wang, W. Guo, D. D. Qu, X. J. Peng, A. Hagfeldt, M. Gratzel and T. L. Ma, *J. Am. Chem. Soc.*, 2012, 134, 3419-3428.
12. E. Ramasamy, C. Jo, A. Anthonysamy, I. Jeong, J. K. Kim and J. Lee, *Chem. Mater.*, 2012, 24, 1575-1582.
13. G. H. Guai, M. Y. Leiw, C. M. Ng and C. M. Li, *Adv. Energy. Mater.*, 2012, 2, 334-338.
14. M. X. Wu, Y. D. Wang, X. Lin, N. S. Yu, L. Wang, L. L. Wang, A. Hagfeldt and T. L. Ma, *PCCP*, 2011, 13, 19298-19301.
15. M. S. Faber, K. Park, M. Caban-Acevedo, P. K. Santra and S. Jin, *J. Phys. Chem. Lett.*, 2013, 4, 1843-1849.
16. F. Gong, H. Wang, X. Xu, G. Zhou and Z. S. Wang, *J. Am. Chem. Soc.*, 2012, 134, 10953-10958.

17. Y. Duan, Q. Tang, J. Liu, B. He and L. Yu, *Angew. Chem., Int. Ed.*, 2014, 53, 14569-14574.

18. G. S. Selopal, I. Concina, R. Milan, M. M. Natile, G. Sberveglieri and A. Vomiero, *Nano Energy*, 2014, 6, 200-210.

19. M. K. Wang, A. M. Anghel, B. Marsan, N. L. C. Ha, N. Pootrakulchote, S. M. Zakeeruddin and M. Gratzel, *J. Am. Chem. Soc.*, 2009, 131, 15976-15977.

20. Z. S. Yang, C. Y. Chen, C. W. Liu, C. L. Li and H. T. Chang, *Adv. Energy. Mater.*, 2011, 1, 259-264.

21. M. L. Que, W. X. Guo, X. J. Zhang, X. Y. Li, Q. L. Hua, L. Dong and C. F. Pan, *J. Mater. Chem. A*, 2014, 2, 13661-13666.

22. J. Xu, J. Y. Xiao, J. Dong, Y. H. Luo, D. M. Li and Q. B. Meng, *Electrochim. Acta*, 2014, 127, 180-185.

23. C. Y. Lin, C. Y. Teng, T. L. Li, Y. L. Lee and H. S. Teng, *J. Mater. Chem. A*, 2013, 1, 1155-1162.

24. Z. Tachan, M. Shalom, I. Hod, S. Ruhle, S. Tirosh and A. Zaban, *J. Phys. Chem. C*, 2011, 115, 6162-6166.

25. H. C. Sun, D. Qin, S. Q. Huang, X. Z. Guo, D. M. Li, Y. H. Luo and Q. B. Meng, *Energ. Environ. Sci.*, 2011, 4, 2630-2637.

26. H. N. Chen, L. Q. Zhu, H. C. Liu and W. P. Li, *J. Phys. Chem. C*, 2013, 117, 3739-3746.

27. J. Y. Lin, W. Y. Wang, Y. T. Lin and S. W. Chou, *ACS Appl. Mater. Interfaces*, 2014, 6, 3357-3364.

28. H. Yu, H. Bao, K. Zhao, Z. Du, H. Zhang and X. Zhong, *J. Phys. Chem. C*, 2014, 118, 16602-16610.

29. J. H. Guo, Y. T. Shi, C. Zhu, L. Wang, N. Wang and T. L. Ma, *J. Mater. Chem. A*, 2013, 1, 11874-11879.

30. X. J. Zheng, J. H. Guo, Y. T. Shi, F. Q. Xiong, W. H. Zhang, T. L. Ma and C. Li, *Chem. Commun.*, 2013, 49, 9645-9647.

31. X. K. Xin, M. He, W. Han, J. H. Jung and Z. Q. Lin, *Angew. Chem., Int. Ed.*, 2011, 50,

11739-11742.

32. J. Xu, X. Yang, Q. D. Yang, T. L. Wong and C. S. Lee, *J. Phys. Chem. C*, 2012, 116, 19718-19723.

33. S. K. Swami, N. Chaturvedi, A. Kumar, N. Chander, V. Dutta, D. K. Kumar, A. Ivaturi, S. Senthilarasu and H. M. Upadhyaya, *PCCP*, 2014, 16, 23993-23999.

34. M.-S. Fan, J.-H. Chen, C.-T. Li, K.-W. Cheng and K.-C. Ho, *J. Mater. Chem. A*, 2015, 3, 562-569.

35. J. Xu, X. Yang, Q. D. Yang, W. J. Zhang and C. S. Lee, *ACS Appl. Mater. Interfaces*, 2014, 6, 16352-16359.

36. Y. Peng, J. Zhong, K. Wang, B. F. Xue and Y. B. Cheng, *Nano Energy*, 2013, 2, 235-240.

37. M. Seol, D. H. Youn, J. Y. Kim, J. W. Jang, M. Choi, J. S. Lee and K. Yong, *Adv. Energy. Mater.*, 2014, 4, 1300775.

38. T. L. Zhang, H. Y. Chen, C. Y. Su and D. B. Kuang, *J. Mater. Chem. A*, 2013, 1, 1724-1730.

39. J. Idigoras, E. Guillen, F. J. Ramos, J. A. Anta, M. K. Nazeeruddin and S. Ahmad, *J. Mater. Chem. A*, 2014, 2, 3175-3181.

40. L. Kavan, J. H. Yum, M. K. Nazeeruddin and M. Gratzel, *ACS Nano*, 2011, 5, 9171-9178.

41. L. Kavan, J. H. Yum and M. Gratzel, *ACS Nano*, 2011, 5, 165-172.

42. M. H. Deng, Q. X. Zhang, S. Q. Huang, D. M. Li, Y. H. Luo, Q. Shen, T. Toyoda and Q. B. Meng, *Nano. Res. Lett.*, 2010, 5, 986-990.

43. R. Toledano, R. Shacham, D. Avnir and D. Mandler, *Chem. Mater.*, 2008, 20, 4276-4283.

44. C. Shen, L. D. Sun, Z. Y. Koh and Q. Wang, *J. Mater. Chem. A*, 2014, 2, 2807-2813.

45. M. Krunks and E. Mellikov, *Optical Organic and Inorganic Materials*, 2001, 4415, 60-65.

46. D. H. Webber and R. L. Brutchey, *J. Am. Chem. Soc.*, 2013, 135, 15722-15725.

47. L. H. Hu, S. Y. Dai, J. Weng, S. F. Xiao, Y. F. Sui, Y. Huang, S. H. Chen, F. T. Kong, X. Pan, L. Y. Liang and K. J. Wang, *J. Phys. Chem. B*, 2007, 111, 358-362.

48. H. Lee, M. K. Wang, P. Chen, D. R. Gamelin, S. M. Zakeeruddin, M. Gratzel and M. K. Nazeeruddin, *Nano Lett.*, 2009, 9, 4221-4227.

49. P. D. Antunez, D. A. Torelli, F. Yang, F. A. Rabuffetti, N. S. Lewis and R. L. Brutchey, *Chem. Mater.*, 2014, 26, 5444-5446.

50. J. D. Roy-Mayhew, D. J. Bozym, C. Punckt and I. A. Aksay, *ACS Nano*, 2010, 4, 6203-6211.

51. D. Menshykau and R. G. Compton, *Electroanalysis*, 2008, 20, 2387-2394.

52. W. J. Wang, X. Pan, W. Q. Liu, B. Zhang, H. W. Chen, X. Q. Fang, J. X. Yao and S. Y. Dai, *Chem. Commun.*, 2014, 50, 2618-2620.

53. T. Loucka, *J. Electroanal. Chem.*, 1972, 36, 355-367.

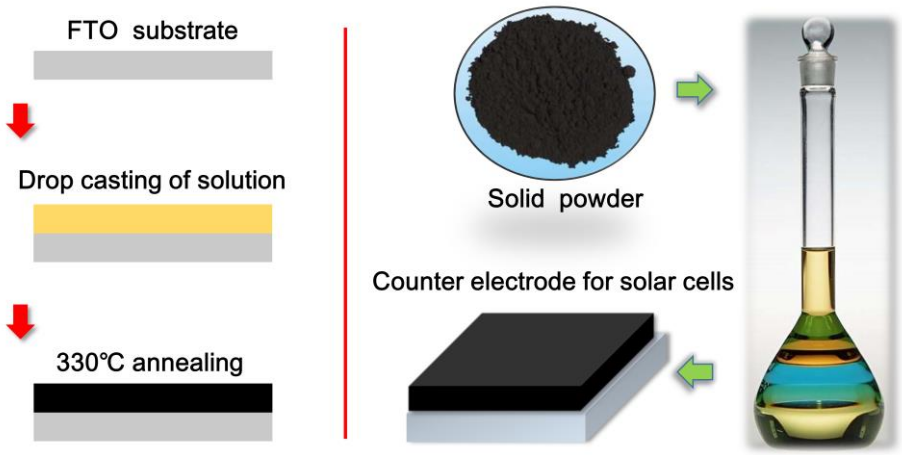

TOC

Solution-deposited chalcogenide films show better catalytic performance than platinum-loaded electrode in both iodide/triiodide ($FeSe_2$) and polysulfide ($Cu_{1.8}S$, CuSe) redox systems.